# A Simplified Dynamic Model of Parachute Inflation

Dean Wolf*
*Sandia Laboratories, Albuquerque, N. Mex.*

**This paper describes a dynamic inflation model for parachutes which predicts increased dimensionless inflation times and increased dimensionless inflation forces observed at high altitudes. As altitude is increased, greater relative parachute inertia results in increased inflation times, and greater relative total system inertia results in increased maximum inflation forces. The effect of Mach number on inflation force is also predicted by the inflation model.**

## Nomenclature

$B_r$ = radial apparent mass coefficient
$B_x$ = axial apparent mass coefficient
$C_D$ = drag coefficient
$C_R$ = radial force coefficient
$D_0$ = parachute constructed diameter
$F$ = vector force
$F_D$ = drag force
$F_R$ = radial force
$Fr$ = Froude number
$F_x$ = axial force
$f_x$ = dimensionless axial force
$f_{x0}$ = maximum value of $f_x$
$g$ = gravitational acceleration
$h$ = altitude
$k$ = mass ratio
$L_s$ = suspension line length
$M$ = Mach number
$m$ = mass
$m_{ci}$ = mass of inflated portion of canopy
$m_r$ = radial apparent mass
$m_x$ = axial apparent mass
$q$ = dynamic pressure
$R_c$ = canopy radius
$r_c$ = $R_c/R_p$
$R_p$ = fully inflated canopy radius
$R_0$ = $D_0/2$
$S$ = area, $\pi R^2$
$t$ = time
$t_*$ = $tV_0/R_p$
$t_{i*}$ = $t_*$ required for inflation
$V_0$ = system initial velocity
$X$ = vector distance
$X$ = distance along flight path
$x$ = $X/R_p$
$x_0$ = $(L_s + R_0)/R_p$
$\gamma$ = trajectory angle
$\theta$ = suspension line half angle
$\rho$ = atmospheric density

*Subscripts*

$c$ = canopy
$f$ = forebody
$p$ = parachute
$t$ = total system

Presented as Paper 73-450 at the AIAA 4th Aerodynamic Deceleration Systems Conference, Palm Springs, Calif., May 21-23, 1973; submitted May 5, 1973; revision received October 29, 1973. This work was supported by the U.S. Atomic Energy Commission.

Index categories: Aircraft Deceleration Systems; Entry Deceleration Systems and Flight Mechanics (e.g., Parachutes).

*Member of Technical Staff, Deceleration and Recovery Systems Division, Aerodynamics Projects Department. Member AIAA.

## Introduction

MOST existing analytical models which describe the inflation of a parachute have coupled solutions to ballistic flight-path equations of motion with largely empirical methods of determining inflation rate. Inflation rate is generally obtained by solving a conservation of mass equation for the inflating canopy internal volume. This is accomplished either by assuming a relationship for the net flow into a canopy as in the analyses of Scheubel,[1] O'Hara,[2] or Heinrich,[3] or by assuming that inflated shape is a function only of distance traveled, as French,[4] Rust,[5] or McEwan[6] have proposed. Although these methods can provide accurate results, they are inherently restricted in application by the empirical use of conservation of mass equation to describe the radial motion of a parachute canopy during inflation. The rate at which mass accumulates inside a parachute canopy is a consequence of the inflation rate and not the sole cause of it.

Solutions generated by these methods are in effect dynamically similar solutions because canopy momentum relations are not utilized. A potentially serious limitation is imposed on the use of the empirical models by the absence of any means of determining when the required conditions for dynamic similarity are satisfied or even what the important similarity parameters are.

A more general approach to the problem is to solve a set of parachute momentum equations, just as momentum equations are solved to describe the system motion along its flight path. Only a few attempts have been made to determine inflation rate by solving parachute momentum equations. A most notable early attempt by Weinig[7] presents a canopy radial equation of motion which contains both fluid and canopy inertia effects and a quasi-steady radial forcing term. The form of the fluid inertia effects was determined by examining the solution for potential flow about an expanding, decelerating sphere. Because the resulting equations contained many unknown coefficients, solutions were not presented. A dynamic inflation model proposed by Toni[8] utilizes a radial momentum equation which contains canopy material inertia and a quasi-steady force but does not include the fluid inertia effects shown to be very significant in an early paper by von Karman.[9] A recent paper by Roberts[10] has modeled an inflating parachute as a continuous elastic system with pressure distributions derived from solutions for potential flow about an expanding, decelerating parabolic shell. Although Robert's work represents the most advanced dynamic inflation model proposed at this time, a single degree of freedom canopy model similar to Weinig's has been chosen for this analysis.

The purpose of this paper is to present the derivation of

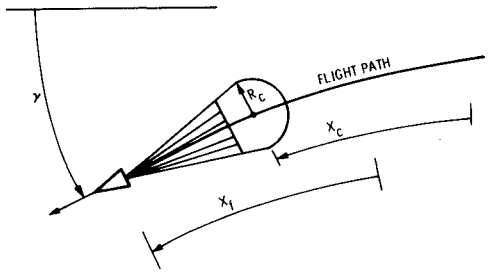


**Fig. 1 Trajectory coordinates.**

equations for a simplified inflation model and a comparison of solutions to the equations with available inflation data. Even though the highly simplified model neglects many details of the inflation process, it provides some insight into the effects of canopy inertia on parachute inflation time. As additional canopy degrees of freedom are added, as in the paper by McVey and Wolf,[11] the result should approach Robert's continuous model without some of the geometric and mathematical difficulties.

## Equations of Motion

As previously proposed by Berndt[12] and French,[13] the parachute inflation sequence is divided into two identifiable phases. During the initial phase, the canopy fills from the skirt until a small region near the vent becomes inflated. The second phase occurs as the inflated portion expands to assume its fully inflated shape. This analysis is concerned only with the second or final inflation phase.

Figure 1 illustrates the trajectory coordinates for the system being considered. The forebody is assumed to be a point mass which develops negligible aerodynamic forces. The forebody and parachute are assumed to possess a common axis of symmetry and to follow the same ballistic path. Relative velocity along the flight path between the parachute and forebody is accounted for, and the canopy shape is described by a single radial degree of freedom.

Figure 2 illustrates the assumed parachute geometry. The parachute is approximated by a cone-sphere with the inflated portion extending forward of the point of maximum diameter as shown. All suspension line and canopy materials are assumed to be inelastic.

The fundamental momentum equation utilized is that derived for a system of variable mass by Thomson[14]

$$m\frac{d^2\bar{X}}{dt^2} = \bar{F} + \frac{dm}{dt}\left(\frac{d\bar{X}_e}{dt} - \frac{d\bar{X}}{dt}\right) \tag{1}$$

where $d\bar{X}_e/dt$ is the absolute velocity of mass entering the system.

If Eq. (1) is used, the equations of motion for the forebody and parachute taken tangent to the flight path become

$$(m_f + m_p - m_{ci})\frac{d^2X_f}{dt^2} = (m_f + m_p - m_{ci})g\sin\gamma - F_x \tag{2}$$

$$(m_{ci} + m_x)\frac{d^2X_c}{dt^2} = m_{ci}g\sin\gamma + F_x - C_D q_c S_c + \frac{dm_{ci}}{dt}\left(\frac{dX_f}{dt} - \frac{dX_c}{dt}\right) - \frac{dm_x}{dt}\frac{dX_c}{dt} \tag{3}$$

Conservation of momentum normal to the flight path yields the equation for rate of change of trajectory angle

$$(m_f + m_p + m_x)\frac{dX_f}{dt}\frac{d\gamma}{dt} = (m_f + m_p)g\cos\gamma \tag{4}$$

The assumption required to make both the forebody and parachute follow the same ballistic path is that in the trajectory angle equation they both possess the same tangential velocity, taken here to be the forebody velocity.

As previously noted, the radial motion of the parachute canopy is described by a single equation

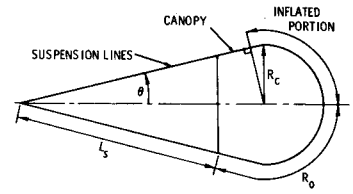


**Fig. 2 Parachute geometry.**

$$(m_{ci} + m_r)\frac{d^2R_c}{dt^2} = 2C_R q_c S_c \sin\theta - F_x \tan\theta - \left(\frac{dm_{ci}}{dt} + \frac{dm_r}{dt}\right)\frac{dR_c}{dt} \tag{5}$$

Use of a single radial degree of freedom restricts the simplified inflation model to unreefed parachutes. Additional degrees of freedom are required[11] to describe reefed parachute inflations. Inspection of the two canopy momentum equations, Equations (3) and (5), shows that they each contain a quasi-steady aerodynamic force, a suspension line force component, and unsteady aerodynamic force terms expressed as fluid inertia or apparent mass effects. The reference area for the quasi-steady radial force is the area of the inflated portion of the canopy of the maximum diameter, because the steady pressure distribution must integrate to give zero radial force aft of this point. Mass terms in Eqs. (3) and (5) should be interpreted as the canopy and apparent mass associated with the inflated portion of the canopy only.

An additional equation is required to provide the constant length constraint imposed by the inelastic material assumption. The distance along a ray of the conical surface shown in Fig. 2 is given by

$$(X_f - X_c)^2 + R_c^2 = \left(L_s + R_0 - \frac{\pi R_c}{2}\right)^2 \tag{6}$$

## Dimensionless Equations

In order to facilitate a parametric study, all equations are reduced to a dimensionless form which is also convenient for obtaining digital computer solutions. Initial velocity, $V_0$, and canopy projected radius at full inflation, $R_p$, are used to reduce the equations to dimensionless form. Dimensionless lengths are represented by lower case letters $x$ and $r$ and dimensionless time by $t_*$.

Dimensionless parameters to be introduced include:

Froude number

$$Fr = V_0/(gR_p)^{1/2}$$

Dimensionless parachute force

$$f_x = (F_x/q_0 S_p)$$

Forebody and parachute mass ratios:

$$k_f = \frac{3m_f}{4\rho\pi R_p^3}; \quad k_p = \frac{3m_p}{4\rho\pi R_p^3}$$

Parachute canopy mass ratio

$$k_c = (k_p m_c/m_p)$$

Total system mass ratio

$$k_t = k_f + k_p$$

Apparent mass coefficients for linear and radial acceleration of the parachute canopy

$$B_x = \frac{3m_x}{4\rho\pi R_c^3}; \quad B_r = \frac{3m_r}{4\rho\pi R_c^3}$$

Parachute quasi-steady drag and radial force coefficients:

$$C_D = \frac{F_D}{q_c S_c}; \quad C_R = \frac{F_R}{2q_c S_c \sin\theta}$$

Table 1. Inflation data for different types of parachutes

| Type/symbol | $D_0(m)$ | $h(km)$ | $M$ | $k_t$ | $k_p$ | $t_i*$ | $f_{x0}$ | Reference |
|---|---|---|---|---|---|---|---|---|
| Disk-gap-band/O | 9.14 | 39.2 | 1.56 | 180 | 20 | 39[a] | 1.18 | 15 |
| | 12.19 | 42.7 | 1.91 | 134 | 16 | 38 | 1.10 | 15 |
| | 12.19 | 48.7 | 2.72 | 328 | 40 | 57 | 1.40 | 15 |
| | 19.72 | 39.2 | 1.59 | 45 | 6.5 | 25.5 | 1.08 | 15 |
| | 12.19 | 51.1 | 3.31 | 492 | 56 | 88 | 0.80 | 16 |
| | 1.68 | — | 2.0 | ∞ | 17 | 40 | 1.2 | 17 |
| | 1.68 | — | 3.0 | ∞ | 24 | 52 | 0.72 | 17 |
| | 4.57 | 0 | 0.04 | ∞ | 0.14 | 10 | — | 18 |
| | 9.14 | 0 | 0.1 | 0.62 | 0.09 | — | 0.096 | 15 |
| | 9.14 | 0 | 0.1 | 0.62 | 0.09 | — | 0.076 | 15 |
| | 12.19 | 3.2 | 0.35 | 0.55 | 0.05 | — | 0.097 | 19 |
| Ringsail/□ | 9.51 | 37.3 | 1.39 | 114 | 9 | 32 | 1.12 | 15 |
| | 16.61 | 39.2 | 1.6 | 75 | 7 | 32 | 1.60 | 15 |
| | 12.19 | 50.4 | 2.95 | 411 | 52 | 96 | 0.91 | 20 |
| | 4.57 | 0 | 0.04 | ∞ | 0.14 | 18 | — | 18 |
| Hemisflo/△ | 1.25 | 25.2 | 2.4 | $10^4$ | 60 | 91 | 1.05 | 21 |
| | 1.25 | 33.1 | 3.44 | $10^5$ | 214 | 248 | 1.39 | 21 |
| Hyperflo/X | 0.82 | 30.6 | 2.8 | $10^5$ | 200 | 110 | 1.10 | 21 |
| | 1.13 | 37.2 | 2.8 | $10^5$ | 265 | 162 | 0.79 | 21 |
| | 1.13 | 26.3 | 3.22 | $10^4$ | 72 | 104 | 0.98 | 21 |
| | 1.13 | 37.4 | 3.98 | $10^5$ | 418 | 293 | 0.67 | 21 |
| | 0.67 | 2.1 | 2.71 | $10^4$ | 38 | 39 | 1.75 | 22 |
| Parasonic/▽ | 1.33 | 23.9 | 2.69 | $10^4$ | 213 | 178 | 2.23 | 23 |
| | 1.33 | 17.2 | 1.48 | $10^3$ | 74 | 121 | 1.88 | 23 |
| | 1.33 | — | 2.8 | ∞ | 152 | 125 | — | 24 |
| Extended skirt/+ | 9.36 | — | — | 4.6 | — | — | 1.1 | 25[b] |
| | 9.75 | — | — | 1.05 | — | — | 0.24 | 25 |
| | 10.67 | — | — | 0.78 | — | — | 0.15 | 25 |

[a] All disk-gap-band inflation times are corrected to an initial radius of $r_c = 0.25$.
[b] Typical average values taken from a large collection of data.

An additional simplifying assumption, that canopy mass per unit area is constant, is made at this point so that $m_{ci} = m_c(R_c/R_p)^2$.

When the suspension line force component is eliminated by adding Eqs. (2) and (3) the forebody acceleration tangent to the flight path is obtained.

$$(k_t - k_c r_c^2)\frac{d^2x_f}{dt_*^2} = \frac{k_t \sin\gamma}{Fr^2} - \frac{3}{8}C_D r_c^2 \left(\frac{dx_c}{dt_*}\right)^2 - (k_c r_c^2 + B_x r_c^3)\frac{d^2x_c}{dt_*^2} - 3B_x r_c^2 \frac{dr_c}{dt_*}\frac{dx_c}{dt_*} + 2k_c r_c \frac{dr_c}{dt_*}\left(\frac{dx_f}{dt_*} - \frac{dx_c}{dt_*}\right) \quad (7)$$

Canopy acceleration along the flight path is obtained by twice differentiating Eq. (6) to obtain

$$\frac{d^2x_c}{dt_*^2} = \frac{d^2x_f}{dt_*^2} + \frac{f_1}{2f_2}\frac{d^2r_c}{dt_*^2} + \frac{1}{4}\left\{\frac{f_1^2}{f_2^3} - \frac{(\pi^2-4)}{f_2}\right\}\left(\frac{dr_c}{dt_*}\right)^2 \quad (8)$$

where

$$f_1 = \pi\left(x_0 - \frac{\pi r_c}{2}\right) + 2r_c$$

$$f_2 = \left\{\left(x_0 - \frac{\pi r_c}{2}\right)^2 - r_c^2\right\}^{1/2}$$

$$x_0 = \frac{(L_s + R_0)}{R_p}$$

Radial acceleration of the canopy is obtained from Eq. (5).

$$(k_c r_c^2 + B_r r_c^3)\frac{d^2r_c}{dt_*^2} = \frac{3}{4}C_R r_c^2 \left(\frac{dx_c}{dt_*}\right)^2 \sin\theta - (2k_c r_c + 3B_r r_c^2)\left(\frac{dr_c}{dt_*}\right)^2 - \frac{3}{8}f_x \tan\theta \quad (9)$$

where Eq. (2) provides $f_x$ as

$$f_x = \frac{8}{3}(k_t - k_c r_c^2)\left(\frac{\sin\gamma}{Fr^2} - \frac{d^2x_f}{dt_*^2}\right)$$

The final dimensionless equation for rate of change of trajectory angle is provided by Eq. (4):

$$Fr^2(k_t + B_x r_c^3)\frac{dx_f}{dt_*}\frac{d\gamma}{dt_*} = k_t \cos\gamma \quad (10)$$

Equations (7-10) provide a set of simultaneous ordinary differential equations solvable for the variables $x_f$, $x_c$, $r_c$, and $\gamma$ as a function of $t_*$.

## Comparison with Data

The dimensionless parameters which appear in the equations of motion give an indication of the types of problems that can be studied with the simplified dynamic model. The effects on the inflation process of the various mass ratios, quasi-steady force coefficients, fluid inertia coefficients, and other parameters could all, at least in theory, be investigated. However, because of the lack of quantitative data available on some of the coefficients in the equations, only approximate effects and trends caused by some of the more important parameters are investigated. The parameters chosen include parachute mass ratio, total system mass ratio, and Mach number.

In order to test the dynamic inflation model, inflation data for several different types of parachutes taken over a wide range of altitudes and Mach numbers were compiled. The data are presented in Table 1. A good deal of scatter exists in some of the data, primarily as a result of the very severe high-speed environment under which the data were obtained. In particular, the inflation times for the smaller parachutes tested at high speeds were very short, so that small absolute measurement errors could result in large

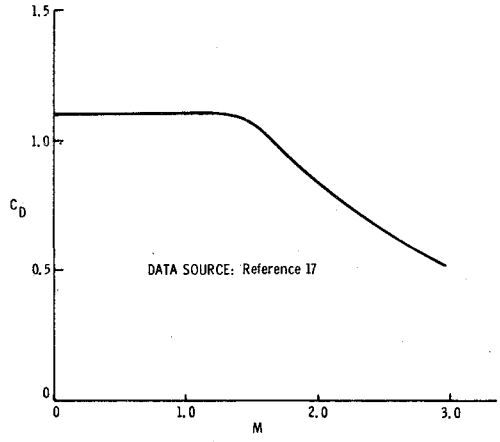


**Fig. 3 Drag coefficient for disk-gap-band-parachute.**

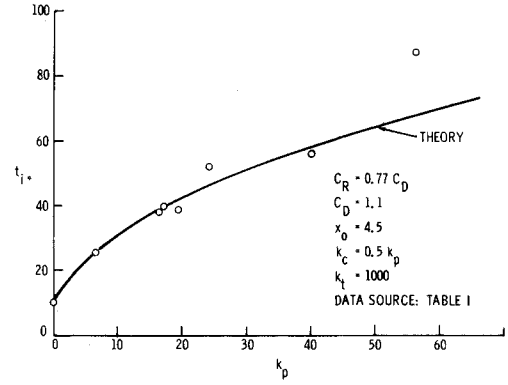


**Fig 4 Variation of inflation time with parachute mass ratio for disk-gap-band parachutes.**

relative errors. Also, at high speeds, both the inflation time and force can be significantly influenced by the deployment method used. The simplified initial conditions assumed for the dynamic model may not always have been appropriate. In addition to the actual data scatter, some errors were undoubtedly introduced by estimating the weights of parachutes for which weight data were not available in the literature. Inflated shape data were not always available either, so the approximate conversion factors of $R_p = 0.35\ D_0$ and $S_p = 0.5\ S_0$ were used for flat and conical parachutes when necessary. The data do cover a wide range of mass ratios and Mach numbers, however, so they are considered adequate for the type of approximate parametric study being conducted here.

The most directly useful set of inflation data is that measured by NASA/LRC for the disk-gap-band parachute. Not only were the data obtained from the use of large parachutes over a wide range of mass ratios and Mach numbers, but radius and force vs time during inflation and parachute weight data are available in the literature. The disk-gap-band data were therefore used exclusively in the initial part of the data comparison.

Of the coefficient data required for the inflation model, drag coefficient data are the most readily available in the literature. Figure 3 shows the drag coefficient vs Mach number variation presented by Bobbitt and Mayhue[17] for the disk-gap-band parachute. The drag coefficients are based on a subsonic projected area ($S_p = 0.5\ S_0$) and hence are double the values often quoted in the literature. Nearly all of the reduction in drag coefficient at supersonic speeds evident in Fig. 3 results from the reduction in average projected area of the parachute as Eckstrom[20] and others have observed. A drag coefficient based on the true projected area would thus be nearly constant over the Mach number range shown. The absence of a drag rise, as Fredette[26] has pointed out, is caused by the formation of an oblique shock pattern forward of the canopy in supersonic flow, which causes a parachute to behave like a more slender body in supersonic than in subsonic flow. The assumption of a normal shock forward of the canopy as Greene[27] and others have assumed would obviously produce an effect which has not been observed, namely, a large increase in parachute drag coefficient at supersonic speeds.

Accurate estimates of radial force coefficients are difficult to obtain because little pressure distribution data for parachutes exist. Wind tunnel tests of ribbon parachutes[28] have shown that the maximum pressure across a canopy occurs near the point of maximum radius and reduces to zero at the point where the inflated portion of the canopy ends. Therefore, the radial force coefficient should exceed one-half the drag coefficient. Inspection of Eq. (9) for the steady-state condition shows that this must be the case or the outward radial force will not exceed the inward component of the suspension line force, and the parachute will collapse. Actual values of the radial force coefficient were extracted from inflation time data as described later.

Fluid inertia or apparent mass effects have received much attention in the parachute literature in recent years. Ibrahim[29] has calculated a value of $B_x = 1$ for a hemispherical shell in potential flow. He has also shown experimentally[30] that geometric porosity has a strong effect in reducing the fluid inertia coefficients. No calculations of the radial inertia coefficient introduced into the dynamic model have been made. The value $B_r = 3$ for a solid sphere is well known (see Milne-Thomson[31]); but because a parachute resembles a hemispherical tension shell, a smaller value would seem appropriate. The assumed value of $B_r = 2$ for an imporous parachute represents little more than a guess. To account for porosity effects, both coefficients were reduced by 50% to values of $B_x = 0.5$ and $B_r = 1$ for the parametric analysis.

Froude number effects were not investigated in this study, because the effects are negligible for essentially all of the tests in Table 1. The effects of Froude number in shaping the trajectory are important when small Froude numbers and large system mass ratios are combined, for example, when very heavily loaded parachutes are deployed at low speeds. Since these conditions were not of interest, a value of $Fr = 100$ was assumed throughout the analysis.

Simplified initial conditions for the equaitons of motion were used to generate numerical solutions

$$(dx_f(0)/dt_*) = (dx_c(0)/dt_*) = 1$$

$$(dr_c(0)/dt_*) = \gamma(0) = 0$$

$$r_c(0) = 0.25$$

The initial radius of $r_c = 0.25$ was typical of the projected radius at bag strip for the disk-gap-band tests. Some initial radial velocity is also evident in the data, but no methods of predicting the velocity was determined. The net effect is that a slightly larger radial force coefficient is required to achieve a particular inflation time than if the proper initial velocity were used.

The purpose of the first parametric study was to establish the variation of dimensionless inflation time with parachute mass ratio for an infinite system mass condition ($k_t$ very large). Such a system does not decelerate appreciably; therefore, the dimensionless inflation time is very nearly equal to the dimensionless inflation distance. Any variation in dimensionless inflation time with $k_p$ therefore represents a violation of the dynamic similarity conditions required for constant distance theory[4] to hold. Solutions to the equations of motion are compared with disk-gap-band inflation data in Fig. 4. A value of radial force coefficient of $C_R = 0.77\ C_D$ was selected to fit the low-altitude subsonic data, for which $k_p$ is very small. By

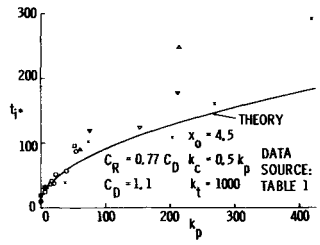


**Fig. 5 Variation of inflation time with parachute mass ratio for different parachutes.**

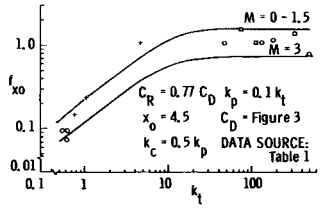


**Fig. 6 Variation of inflation force with system mass ratio and Mach number.**

varying only $k_p$, the curve in Fig. 4 was obtained. A suspension line length of one constructed diameter and a canopy mass of one-half the parachute mass were assumed. Close agreement between data and prediction was obtained. Note that, for any particular parachute, an increase in $k_p$ can only be accomplished by decreasing atmospheric density or increasing altitude. The increase in inflation time (or distance) apparent in Fig. 4 is thus a direct altitude effect. That such an effect must exist was pointed out by Fredette:[26] at high altitudes, the inertia of the parachute becomes relatively greater; therefore, it inflates more slowly.

In that the inflation times predicted with subsonic force coefficients are in close agreement with data taken over a wide Mach number range, the actual effect of Mach number on inflation time is thought to be small. This is consistent with the previous observation that the average pressure coefficient across the canopy changes little with Mach number.

Figure 5 shows the same variation as Fig. 4, but with data for several different types of parachutes added to extend the range of $k_p$. The previously mentioned data scatter is evident in the tests of small parachutes conducted at high speeds. However, the same general trend seems to hold. Most of the data points in Fig. 5 fall above the curve predicted for the disk-gap-band parachutes. A large part of the observed increased in inflation time is caused by the larger porosity of the other parachutes. In that the disk-gap-band inflates as rapidly as a solid canopy,[18] the predicted curve should represent a minimum inflation time for low porosity parachutes. Sufficient data do not exist at this time to accurately predict the effect of porosity.

A brief investigation of the effects of total system mass ratio and Mach number on maximum inflation force is summarized in Fig. 6. As von Karman,[9] French,[25] Whitlock and Bendura,[15] and Ewing[32] have shown, maximum force is a function of total system mass ratio. For small mass ratios, the system decelerates significantly during inflation, and the lower velocity results in a lower maximum force. The direct effect of increasing altitude is obtained by moving from lower to higher mass ratios, and hence increasing maximum dimensionless force. A Mach number correction was applied by varying drag coefficient according to the data of Fig. 3. The dynamic inflation model predicts the trend with mass ratio reasonably well, and the Mach number correction seems to bracket the data points.

## Conclusions

A simplified dynamic inflation model for parachutes which removes some of the empirical restrictions of previous models has been derived. The model predicts reasonably well the effects of altitude on parachute inflation time and force when compared with available test data. Dimensionless inflation time is shown to increase with altitude as the parachute inertia becomes relatively greater than that of the surrounding air. Dimensionless force also increases with altitude as the total system inertia becomes relatively greater. Independent calculation or measurement of the force coefficients appearing in the model is required to accurately predict porosity and Mach number effects.

## References

[1]Scheubel, F. N., "Notes on Opening Shock of a Parachute," ATI No. 34073, April 1946, Wright Air Development Center, Ohio.

[2]O'Hara, F., "Notes on the Opening Behavior and the Opening Forces of Parachutes," *Royal Aeronautical Society Journal*, Vol. 53, Nov. 1949, pp. 1053–1062.

[3]Heinrich, H. G., "A Linearized Theory of Parachute Opening Dynamics," *The Aeronautical Journal*, Vol. 76, No. 744, Dec. 1972, pp. 723–731.

[4]French, K. E., "Inflation of a Parachute," *AIAA Journal*, Vol. 1, No. 11, Nov. 1963, pp. 2615–2617.

[5]Rust, L. W., Jr., "Theoretical Investigation of the Parachute Inflation Process," NVR-3887, July 1965, Northrop Corporation, Ventura Division, Newbury Park, Calif.

[6]McEwan, A. J., "An Investigation of Parachute Opening Loads, and a New Engineering Method for Their Determination," AIAA Paper 70-1168, Dayton, Ohio, 1970.

[7]Weinig, F. S., "On the Dynamics of the Opening Shock of a Parachute," TR-6, Feb. 1951, USAF Office of Aeronautical Research, Wright Air Development Center, Ohio.

[8]Toni, R. A., "Theory on the Dynamics of a Parachute System Undergoing Its Inflation Process," AIAA Paper 70-1170, Dayton, Ohio, 1970.

[9]von Kármán, T., "Note on Opening Shock of Parachutes at Various Altitudes," ATI 200-814, 1945,

[10]Roberts, B. W., "The Aerodynamic Inflation of Shell Type Structures with Particular Reference to Parachutes," *Royal Aeronautical Society Symposium on Parachutes and Related Technologies*, Sept. 1971, London.

[11]McVey, D. F. and Wolf, D. F."Analysis of Deployment and Inflation of Large Ribbon Parachutes," AIAA Paper 73-451, Palm Springs, Calif., 1973.

[12]Berndt, R. J., "Experimental Determination of Parameters for the Calculation of Parachute Filling Times," *Jahrbuck 1964 der WGLR*, Vieweg & Son, Braunschweig, 1965, pp. 299–316.

[13]French, K. E., "The Initial Phase of Parachute Inflation," *Journal of Aircraft*, Vol. 6, No. 1, July-Aug. 1969, pp. 376–378.

[14]Thomson, W. T., *Introduction to Space Dynamics*, John Wiley and Sons, Inc., New York, 1961, pp. 220–221.

[15]Whitlock, C. H. and Bendura, R. J., "Inflation and Performance of Three Parachute Configurations for Supersonic Flight Tests in a Low-Density Environment," TN D-5296, July, 1969, NASA.

[16]Eckstrom, C. W., "Flight Test of a 40-foot Nominal Diameter Disk-Gap Band Parachute Deployed at a Mach Number of 3.31 and a Dynamic Pressure of 10.6 Pounds per Square Foot," TM-X-1924, Feb. 1970, NASA.

[17]Bobbitt, P. J. and Mayhue, R. J., "Supersonic and Subsonic Wind-Tunnel Tests of Reefed and Unreefed Disk-Gap-Band Parachutes," AIAA Paper 70-1172, Dayton, Ohio, 1970.

[18]Whitlock, C. H., "Wind Tunnel Investigation of Inflation of Disk-Gap-Band and Modified Ringsail Parachutes at Dynamic Pressures Between 0.24 and 7.07 Pounds per Square Foot," TM-X-1786, May 1969, NASA.

[19]Murrow, H. N and Eckstrom, C. V., "Performance of Disk-Gap-Band, Ringsail, and Cross Parachutes at Low Earth Altitudes," *Journal of Spacecraft and Rockets*, Vol. 8, No. 4, April 1971, pp. 418–420.

[20]Eckstrom, C. V., "High-Altitude Flight Test of a 40-Foot Diameter Ringsail Parachute at a Deployment Mach Number of 2.95," TN-D-5796, June 1970, NASA.

[21]Nickle, W. E. and Sims, L. W., "Study and Exploratory Free-Flight Investigation of Deployable Aerodynamic Decelerators Operating at High Altitudes and at High Mach Numbers," FDL-TDR-64-35, Vol. I, July 1964, Air Force Flight Dynamics Lab., Wright-Patterson Air Force Base, Ohio.

[22]Turner, R. and McMullen, J. C., "Feasibility of Parachute Operation at High Mach Numbers and Dynamic Pressures," AIAA Paper 66-24, New York, 1966.

[23]Bloetscher, F. and Arnold, W. V., "Aerodynamic Deployable Decelerator Performance-Evaluation Program," AFFDL-TR-67-60, October 1967, Air Force Flight Dynamics Lab., Wright-Patterson Air Force Base, Ohio.

[24]MacLanahan, D. A., "An Investigation of Various Types of Decelerators at Mach Number 2.8," AEDC-TR-66-136, July 1966, Arnold Engineering Development Center, Arnold Air Force Station, Tullahoma, Tenn.

[25]French, K. E., "Model Law for Parachute Opening Shock," *AIAA Journal*, Vol. 2, No. 12, Dec. 1964, pp. 2226–2228.

[26]Fredette, R. O., "Parachute Research Above Critical Aerodynamic Velocities," Rept. P-1031C, 1961, Cook Research Laboratories, Morton-Grove, Ill.

[27]Greene, G. C., "Opening Distance of a Parachute," *Journal of Spacecraft and Rockets*, Vol. 7, No. 1, Jan 1970, pp. 98–100.

[28]Dickie, G. D., "Tests of FIST Ribbon Parachutes in the UAC Subsonic Wind Tunnel," United Aircraft Corporation Rept. R-1408-1, Feb. 1959, East Hartford, Conn.

[29]Ibrahim, S. K., "Potential Flowfield and Added Mass of the Idealized Hemispherical Parachute," *Journal of Aircraft*, Vol. 4, No. 2, March-April 1967, pp. 96–100.

[30]Ibrahim, S. K., "Experimental Determination of the Apparent Moment of Inertia of Parachutes," AFFDL-TDR-64-153, April 1965, Air Force Flight Dynamics Lab., Wright-Patterson Air Force Base, Ohio.

[31]Milne-Thomson, L. M., *Theoretical Hydrodynamics*, 5th edition, MacMillan Co., New York, 1968, p. 479.

[32]Ewing, E. G., "Ringsail Parachute Design," AFFDL-TR-72-3, January 1972, Air Force Flight Dynamics Lab., Wright-Patterson Air Force Base, Ohio.

JANUARY J. AIRCRAFT VOL. 11, NO. 1

# A Conceptual Study of Leading-Edge-Vortex Enhancement by Blowing

R. G. Bradley* and W. O. Wray†
*General Dynamics, Fort Worth, Texas*

**A conceptual wind-tunnel-test program has been conducted to verify that blowing a stream of high-pressure air over a swept-wing surface in a direction roughly parallel to the leading edge enhances the vortex system. The blowing is shown to intensify the leading-edge vortex and thus delay the deleterious effects of vortex breakdown to higher angle of attack. As a result, the vortex-lift is significantly increased and, as the blowing rate is increased, appears to approach the value predicted by the Polhamus suction-analogy for thin wings.**

## Nomenclature

$AR$ = aspect ratio
$C$ = wing root chord
$C_w$ = root chord of theoretical trapezoidal wing
$C_D$ = drag coefficient
$C_L$ = lift coefficient
$C_M$ = moment coefficient about ¼ MAC
$C_\mu$ = momentum coefficient
$C_{Do}$ = zero-lift drag coefficient
$\alpha$ = angle-of-attack

## Introduction

DESIGN concepts that take advantage of vortex lift play an important part in improving maneuverability of current air-superiority fighters. Further, takeoff and landing performance of other advanced aircraft, e.g., supersonic aircraft, rely to a large extent upon favorable leading-edge vortex-induced effects.

The use of concentrated blowing to enhance and strengthen a wing leading-edge-vortex system, of the type illustrated in Fig. 1, can offer significant improvements in lifting efficiency. The stability of a vortex is known to be related to the longitudinal flow along the axis of the vortex. Ringleb[1] noted the importance of the vortex-core flow in early attempts to establish a stationary vortex for flow control. The application of spanwise blowing to increase lift has been described by Cornish,[2] and spanwise flap blowing has been shown by Dixon[3] to increase the flap-lift increment. In flow visualization studies at ONERA, Werle[4] has shown that leading-edge-vortex breakdown can be controlled on delta wings by concentrated blowing along the vortex axis.

Some of the benefits of vortex enhancement are noted in Fig. 1. For wings with high leading-edge sweep, the augmented natural vortex results in an increased vortex-lift increment. For wings with low leading-edge sweep, the blowing aids in the formation of the leading-edge vortex, thus developing vortex lift where none is developed naturally. Vortex breakdown is delayed to higher angles of at-

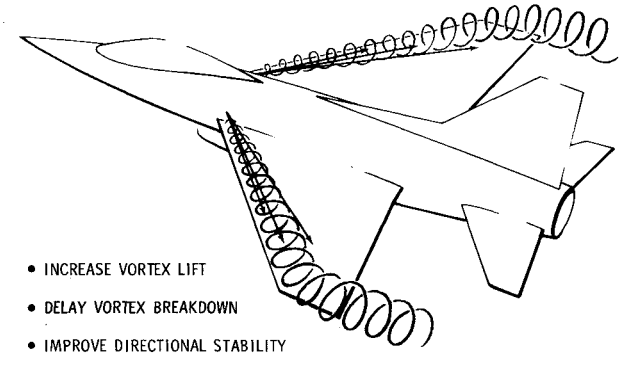


**Fig. 1 Blowing concept for vortex enhancement.**

Presented as Paper 73-656 at the AIAA 6th Fluid and Plasma Dynamics Conference, Palm Springs, Calif., July 16–18, 1973; submitted July 11, 1973.

Index categories: Aircraft Aerodynamics; Subsonic and Transonic Flow.

*Design Specialist, Aerospace Technology Dept., Convair Aerospace Div. Associate Fellow AIAA.

†Senior Aerodynamics Engineer, Aerospace Technology Dept., Convair Aerospace Div.